Scripta Materialia 158 (2019) 121–125

Contents lists available at ScienceDirect

Scripta Materialia

journal homepage: www.elsevier.com/locate/scriptamat

Coalescence mechanism of helium bubble during tensile deformation revealed by *in situ* small-angle X-ray scattering

Jie Gao [a,b], Hefei Huang [a,*], Jizhao Liu [a,b], Jianrong Zeng [a,*], Ruobing Xie [a], Yan Li [a,*]

[a] Shanghai Institute of Applied Physics, Chinese Academy of Sciences, Shanghai 201800, China
[b] University of Chinese Academy of Sciences, Beijing 100049, China

ARTICLE INFO

Article history:
Received 19 June 2018
Received in revised form 23 August 2018
Accepted 28 August 2018
Available online xxxx

Keywords:
Helium bubbles
SAXS
Nickel foil
Tensile stress
Bubble coalescence

ABSTRACT

Helium nanobubbles created in nickel foil under helium ion irradiation are studied using the combination of small-angle X-ray scattering (SAXS) measurement and transmission electron microscopy (TEM) characterization. The log-normal distribution of bubble sizes obtained by SAXS agrees rather well with the TEM results. Under the tensile stress, SAXS experiments were carried out to follow *in situ* the evolution of helium nanobubbles. A detailed analysis revealed that the bubbles performed coalescence *via* the elongation in the direction of tensile stress loading. Our finding demonstrated that bubble "deformation and coalescence" mechanism was also applicable in bubble growth under external stress.

The generation and evolution of helium bubbles in metallic materials has been widely investigated [1–3]. For example, the understanding of bubble evolution mechanisms is of major importance to predict the damages in the structural materials in nuclear reactors [4]. It is well known that the presence of helium bubbles can lead to the degradation of materials, such as the embrittlement [5–7] and swelling [8–10].

Helium bubbles are usually studied using transmission electron microscopy (TEM), which can give us intuitional images showing the bubble distribution, shapes and even the dynamical bubble evolution under heating [11] or stress [12] conditions. Moreover, the quantitative information of helium bubbles at local region, such as number density and mean size, can also be extracted from TEM images. Recently, it was reported that small-angle X-ray scattering (SAXS) experiments were adopted to study the growth and migration of nanobubbles in silicon [13,14]. Using SAXS, the helium density and pressure within the bubbles can be also determined [15]. SAXS experiments allow the investigation of bubble evolution by analyzing the scattering profile contributed from a large bubble population. Therefore, it gives the information of bubble evolution with good statistics. More importantly, the SAXS experiments were not confined to the vacuum environment and metal samples with thickness of several microns can also be penetrated by X-ray with proper energy. As a result, it allows us to perform the *in situ* mechanical experiments on micron-thick samples.

In this study, the bubble size distribution in samples was investigated using both SAXS and TEM techniques. Using SAXS experiments, the bubble evolution under tensile deformation was further revealed by the variation of bubble mean size, number density and total bubble volumes.

The samples used in this study are polycrystalline nickel foils (99.95 wt%) with grain sizes around ~3 μm and thickness of ~2 μm. After the cleaning with a solution of 50% acetone and 50% ethyl alcohol, the samples were annealed at 600 °C for ~30 min in the irradiation chamber before the ion irradiation. Then, they were irradiated by 0.5 MeV helium ions to the dosages of 3×10^{16} and 9×10^{16} ions/cm^2 at 600 °C using a 4 MV Pelletron accelerator. Cross-sectional TEM samples (5 μm × 2 μm) were prepared using a focused ion beam (FIB). The samples were imaged using a Tecnai G2 F20 TEM operated at 200 kV.

In the tensile experiments, the nickel foil irradiated by 9×10^{16} ions/cm^2 ions was made into samples with a narrow center (not ASTM standard) using the laser cutting (Fig. S1(a)). The detailed consideration in the design of sample dimension can be found in *Supplementary material*. The samples with the special shape would be most likely fractured at the center, where the X-ray beam was set to penetrate from that position. The SAXS measurements were carried out in transmission mode on beamline BL16B1 of the Shanghai Synchrotron Radiation Facility (SSRF). The following gives some important equations used in the

* Corresponding authors.
E-mail addresses: huanghefei@sinap.ac.cn (H. Huang), zengjianrong@sinap.ac.cn (J. Zeng), liyan@sinap.ac.cn (Y. Li).

https://doi.org/10.1016/j.scriptamat.2018.08.050
1359-6462/

present data analysis. Other information related to the SAXS measurement and data conversion can be found in *Supplementary material*. The amplitude of the scattering vector q is given by

$$q = 4\pi \sin\theta/\lambda \tag{1}$$

where λ is the X-ray wavelength and θ is the half scattering angle. The integrated intensity Q_0 of the scattered signal can be evaluated as follows:

$$Q_0 = \int_0^\infty I(q)q^2 dq = 2\pi^2(\Delta\rho)^2 f_v(1-f_v) \tag{2}$$

where $I(q)$ is the absolute scattering intensity of a multi-particle system, f_v is the volume fraction and $\Delta\rho$ is the electron density contrast between the scatters and matrix. Here, a new parameter, the volume of helium bubbles per investigated unit surface was introduced as V_{bubble}:

$$V_{bubble} = f_v \times e_{tot} \tag{3}$$

where e_{tot} is the total thickness of the sample. Considering that f_v is far smaller than 1, thus the Eq. (2) can be rewritten as follow:

$$Q_0 \times e_{tot} = 2\pi^2(\Delta\rho)^2 V_{bubble} \tag{4}$$

In practice, the $I \cdot q^2$ *vs.* q plots are commonly used in the interpretation of the SAXS. A family of nano-scatters can be indicated by the existence of a maximum in the $I \cdot q^2$ *vs.* q plot. In first approximation, the position of this maximum is inversely related to their size. In addition, the $I \cdot q^2$ *vs.* q plot can also be used to determine the total integrated intensity Q_0 and thus to estimate the volume fraction of nano-scatters, as suggested by Eq. (4). For highly diluted suspensions of non-aggregated scatters, the structure factor can be taken as unity. For the special case of a sphere the form factor $P(q)$ can be calculated as [16]:

$$P(q) = \left(3\frac{\sin(qr) - qr\cos(qr)}{(qr)^3}\right)^2 \tag{5}$$

In fact, most helium bubbles are polydisperse. Therefore, the measured intensity represents the sum of the scattering intensity from scatters of various sizes

$$I(q) = f_n \int_0^\infty V(r)^2 \cdot N(r) \cdot (\Delta\rho)^2 \cdot P(q) \tag{6}$$

where f_n is the number of nano-scatters per investigated unit volume, $N(r)$ is the number distribution of scatter size that can be given, for example, by a Gaussian or log normal distribution. In this work, a log-normal distribution of bubble sizes was adopted, thus the size distribution can be written as:

$$N(r_i) = \frac{1}{\sqrt{2\pi}\sigma r_i} \exp\left(-\frac{(\ln(r_i/R_{ln})^2}{2\sigma^2}\right) \tag{7}$$

where $N(r_i)$ is the number percentage of bubbles in class i, R_{ln} is the mean value and σ the standard deviation.

The profiles of helium concentration and displacement per atom (dpa) for the 9×10^{16} ions/cm^2 irradiation case were shown in Fig. S2 (a). Helium bubble formation was indicated by underfocus and overfocus TEM images (Fig. S2(b) and (c)). Using SAXS, bubble size and number density in the irradiated samples were measured. Fig. 1(a) shows the raw scattering profiles read by the CCD, including the original sample. Using standard calibration material (glassy carbon), the raw scattering profiles was transformed into the absolute scattering intensity profiles (Fig. 1(b)) after correcting the scattering from the original sample. Compared to the case of the lower dose irradiation, the scattering enhanced obviously in the case of the higher dose irradiation. By plotting the $I \cdot q^2$ *vs.* q profile (Fig. 1(c)), a family of scatters can be induced by the appearance of a peak in each case. The peak located at $q = 0.96$ nm^{-1} in the 3×10^{16} ions/cm^2 case, and it moved towards the left of $q = 0.76$ nm^{-1} in the 9×10^{16} ions/cm^2 case. Using the log-normal size distribution (number distribution of bubble sizes), the plots were fitted and the best fitting curves were also given in Fig. 1 (c) for the comparison purpose. For the lower dose case, the fitting agrees quite well with the experimental profile. As for the higher dose case, the fitting deviated significantly from the experimental profile in

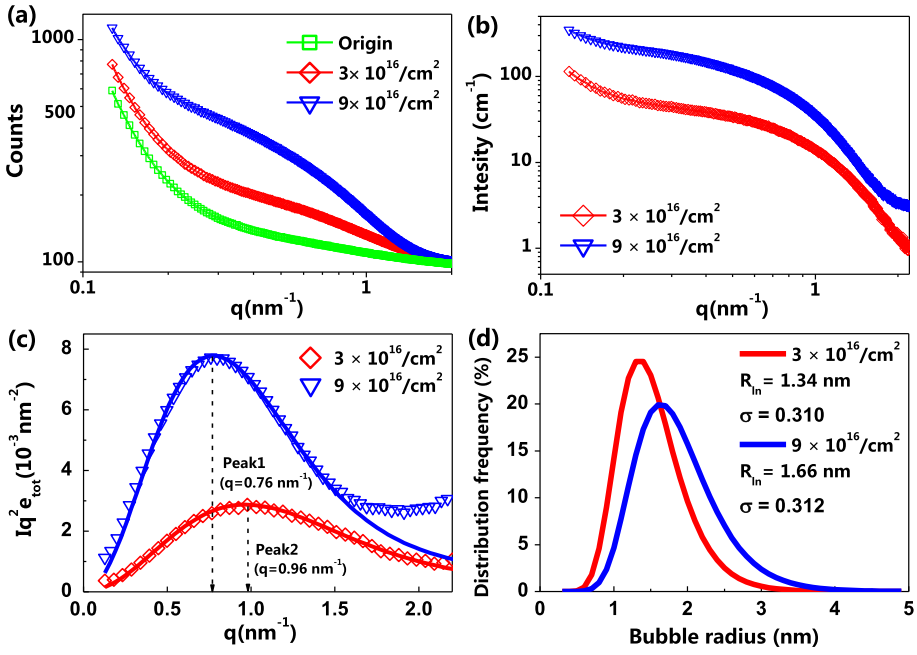

Fig. 1. SAXS experiments on the as-implanted samples. (a) Raw intensity profiles read by the CCD device. (b) Absolute scattering intensity profiles after correcting the contribution from reference sample. (c) SAXS spectra and their best fitting curves obtained using a log-normal size distribution. (d) Bubble size distribution profiles obtained by fitting the SAXS spectra.